ELECTRIC AND MAGNETIC PROPERTIES OF $Ba_{0.97}Ca_{0.03}Ti_{0.94}Sn_{0.06}O_3$-$Mn_{0.85}Ni_{0.15}Zn_{0.15}Fe_2O_4$ MULTIFERROIC CERAMIC COMPOSITES FABRICATED VIA THE SOLID-STATE COMBUSTION TECHNIQUE

Nutkamon Sonchaopria[1], Jirayut Meechob[1], Bhoowadol Thatawong[1], Naratip Vittayakorn[2], Supree Pinitsoontorn[3], Aurawan Rittidech[4], Pongsakorn Jantaratana[5], Suphornphun Chootin[1,6,*] and Theerachai Bongkarn[1,6]

Received: October 27, 2024; Revised: February 01, 2025; Accepted: February 01, 2025

Abstract

Multiferroic composites with the general formula (1-x)($Ba_{0.97}Ca_{0.03}Ti_{0.94}Sn_{0.06}O_3$)-x($Mn_{0.85}Ni_{0.15}Zn_{0.15}Fe_2O_4$) (BCTS/MNZF) (x = 0.1, 0.2, 0.3, 0.4, and 0.5) were prepared using the solid-state combustion method. The structure, morphology, dielectric, ferroelectric, magnetic, and magnetoelectric properties were analyzed. The samples were sintered at 1,300°C for 2 h. The X-ray Diffraction (XRD) patterns revealed tetragonal perovskite, orthorhombic perovskite, and cubic spinel structures corresponding to the BCTS and MNZF phases. Secondary phases (Mn_2O_3 and SnO) appeared in the sintered samples with x>0.2. Increasing MNZF content enhanced ferrite grain growth in the composites. The dielectric constant showed an overall decreasing trend with increasing MNZF content, with a smaller effect at lower frequencies. At lower frequencies, the dielectric constant declined with increasing frequency before stabilizing around 10 kHz. As ferrite content increased, the density, dielectric constant, and magnetoelectric coefficient (α_{ME}) decreased from 5.66 to 5.12 g/cm³, 1388 to 862, and 7.24 to 4.05 mV/cm·Oe, respectively. While the saturation magnetization (M_s) rose substantially from 0.75 to 13.14 emu/g. These findings offer valuable insights into enhancing lead-free multiferroic composite ceramics for targeted applications in magnetoelectric devices.

Keywords: **BCTS-MNZF; Ferroelectric; Ferromagnetic; Multiferroic; Solid-state combustion**

---

[1] *Department of Physics, Faculty of Science, Naresuan University, Phitsanulok, 65000, Thailand. E-mail: researchcmu@yahoo.com; jirayutm68@nu.ac.th; bhoowadolt66@nu.ac.th; suphornphunc@nu.ac.th**
[2] *Advanced Material Research Unit, Faculty of Science, King Mongkut's Institute of Technology Ladkrabang, Bangkok 10520, Thailand. E-mail: naratip.vi@kmitl.ac.th; naratipcmu@yahoo.com*
[3] *Institute of Nanomaterials Research and Innovation for Energy (IN-RIE), Khon Kaen University, Khon Kaen 40002, Thailand. E-mail: psupree@kku.ac.th*
[4] *Department of Physics, Faculty of Science, Mahasarakham University, Mahasarakham, 44150, Thailand. E-mail: aurawan.r@msu.ac.th*
[5] *Department of Physics, Faculty of Science, Kasetsart University, Bangkok 10900, Thailand. E-mail: fscipsj@ku.ac.th*
[6] *Research Center for Academic Excellence in Applied Physics, Faculty of Science, Naresuan University, Phitsanulok, 65000, Thailand. E-mail: suphornphunc@nu.ac.th[*]; theerachaib@nu.ac.th*
[*] *Corresponding author*

DOI: https://doi.org/10.55766/sujst11623

Introduction

Multiferroic composite ceramics are engineered by combining materials with distinct ferroelectric and magnetic properties, allowing multiple ferroic behaviors simultaneously. These materials are valuable for applications such as energy conversion, memory storage, sensors, and actuators (Leung *et al*., 2018; Ortega *et al*., 2015; Scott, 2007). However, single-phase multiferroics with room-temperature ferroelectric and ferromagnetic properties are rare and typically show weak magnetoelectric (ME) coupling, which limits their practical use (Chen *et al*., 2014; Scott, 2013). Two-phase composites integrate significant piezoelectric and magnetostrictive properties, offer strong ME coupling while providing greater design and functional versatility (Navadeepthy *et al*., 2022; Wang *et al*., 2020). Magnetoelectric coupling is typically created by combining magnetic materials like ferrites with piezoelectric (ferroelectric) elements like $BaTiO_3$ or $PbTiO_3$ (Matavž *et al*., 2021).

Lead-free ferroelectric materials based on $BaTiO_3$ (BT) with a perovskite ABO_3 structure, including BaTi, BaCaTi, BaCaTiZr, and BaCaTiSn, have been widely explored due to their excellent dielectric properties and good piezoelectric performance. Recently, Chootin and Bongkarn, (2017) investigated $Ba_{0.97}Ca_{0.03}Ti_{0.94}Sn_{0.06}O_3$ (BCTS) ceramics prepared via the solid-state combustion method. Their findings highlighted that BCTS ceramics displayed both tetragonal and orthorhombic interphases, good morphology with average grain sizes of 12-14 µm, and a maximum density of 5.79 g/cm³. Additionally, the ceramics demonstrated excellent electrical properties (ε_r = 4,951, ε_C = 19,185, P_r = 12.74 µC/cm^2, E_c = 1.60 kV/cm) and good piezoelectric performance (d_{33} = 528 pC/N), highlighting their potential for lead-free applications.

Spinel ferrites have the chemical formula MFe_2O_4, where M represents a divalent metal ion such as Mn^{2+}, Ni^{2+}, Cu^{2+}, Co^{2+}, Zn^{2+} (Dastjerdi *et al*., 2023). Mn-Zn ferrites, in particular, are widely utilized in electronics, including transformer cores, high-frequency inductors, and microwave components, due to their high permeability and excellent magnetic field conductivity, (Thakur *et al*., 2020). The properties of Mn-Zn spinel ferrites have been enhanced by metal substitution to make composites such as $Mn_{0.5}Zn_{0.5}Sc_{0.05}Fe_{1.95}O_4$ (M_s = 31.48 emu/g) (Angadi *et al*., 2017), $Mn_{0.55}Zn_{0.45}Gd_{0.01}Fe_{1.99}O_4$ (M_s = 46.4 emu/g) (Islam *et al*., 2013), $Mn_{0.5}Zn_{0.5}Al_{0.1}Fe_{0.9}O_4$ (M_s = 35 emu/g) (Haralkar *et al*., 2013), and $Mn_{0.5}Zn_{0.5}Sm_{0.5}Fe_{1.5}O_4$ (M_s = 42.10 emu/g) (Yadav *et al*., 2015). Introducing additional nickel (Ni^{2+}) into manganese-zinc (Mn-Zn) ferrites is a purposeful modification aimed at refining and optimizing their properties for particular applications. This adjustment primarily serves to increased electrical resistivity, enhanced magnetic permeability and improved frequency response (Thakur *et al*., 2020). Jalaiah and Babu (2017) synthesized nickel-substituted $Mn_{0.85}Zn_{0.15}Ni_xFe_2O_4$ (x = 0.03, 0.06, 0.09, and 0.15) ferrites using the sol-gel auto-combustion method. The composition with x = 0.15 demonstrated the highest saturation magnetization of 137.246 emu/g. High saturation magnetization materials are critical for designing efficient magnetic systems and have applications in transformers, magnetic sensors, and data storage devices (Verma *et al*., 2006; Latorre-Esteves *et al*., 2009).

Various composites have been explored to enhance the magnetoelectric (ME) effect, focusing on the synthesis of ceramic materials the combine barium titanate with Mn-Zn ferrite spinel perovskites. Examples include $Mn_{0.5}Zn_{0.5}Fe_2O_4$-$Ba_{0.85}Sr_{0.15}Ti_{0.9}Hf_{0.1}O_3$ and $MnZnFe_2O_4$-$BaTiO_3$ (Khader and Sankarappa, 2016; Gao *et al*., 2019). Gao *et al.* (2019) investigated (1-x)$Mn_{0.5}Zn_{0.5}Fe_2O_4$-x$Ba_{0.85}Sr_{0.15}Ti_{0.9}Hf_{0.1}O_3$ composite ceramics with varying x values (0.2, 0.35, 0.5, 0.65, and 0.8). Among these, the composite with x = 0.65, corresponding to a mixture of magnetic and ferroelectric phases, demonstrated a high saturation magnetization (M_s = 32.44 emu/g). However, the magnetoelectric coefficient (α_{ME} = 1.42 mV/cm•Oe) was lower than lead-based composites (α_{ME} = 7.53 mV/cm•Oe) (Fawzi *et al*., 2010). To enhance the magnetoelectric coupling coefficient in composite ceramics with shared perovskite and spinel phases, this study investigates the ME coupling coefficient of (1-x)($Ba_{0.97}Ca_{0.03}Ti_{0.94}Sn_{0.06}O_3$)-x($Mn_{0.85}Ni_{0.15}Zn_{0.15}Fe_2O_4$) (BCTS/MNZF) (x = 0.1, 0.2, 0.3, 0.4, and 0.5) prepared using the solid-state combustion method.

Materials and Method

$Ba_{0.97}Ca_{0.03}Ti_{0.94}Sn_{0.06}O_3$ (BCTS) powder was fabricated by the solid-state combustion method using glycine as the fuel. The raw materials of $Ba(NO_3)_2$ (99.00%; Himedia, Ind), $Ca(NO_3)_2{\cdot}4H_2O$ (99.00%; Ajax, Aust), TiO_2 (99.00%; Kemaus, Aust), and SnO_2 (99.90%; Sigma-Aldrich, Aust) were accurately weighed according to the desired stoichiometric ratio and mixed using a zirconia ball mill in ethanol for 24 h. The resulting suspension was dried at 100°C, then mixed with glycine ($C_2H_5NO_2$) in a 1:2 ratio. The prepared powders were calcined at 1,100°C for 2 h with a heating rate of 5°C/min and allowed to cool down naturally (Chootin and Bongkarn, 2017).

$Mn_{0.85}Ni_{0.15}Zn_{0.15}Fe_2O_4$ (MNZF) powder was synthesized using the solid-state combustion method with glycine as the fuel. The preparation used the raw materials of MnO_2 (99.00%; Sigma-Aldrich, Aust), ZnO (99.00%; Merck, German), NiO (99.00%; Merck, German), and $Fe(NO_3)_3.9H_2O$ (101%; Ajax, Aust). These reagents were precisely weighed according to the required stoichiometry ratio and blended using a ball mill for 24 h. After drying, the resulting powder was combined with glycine in a 1:2 ratio (MZNF to glycine) and calcined at 1,150°C for 2 h.

BCTS/MNZF composites with the general formula (1-x)($Ba_{0.97}Ca_{0.03}Ti_{0.94}Sn_{0.06}O_3$)-x($Mn_{0.85}Ni_{0.15}Zn_{0.15}Fe_2O_4$) were prepared with x values of 0.1, 0.2, 0.3, 0.4, and 0.5. The powders were mixed with 3 wt% polyvinyl butyral (PVB) binder solution and subjected to additional ball milling for 12 h. The resulting powders were dried and shaped into pellets with a diameter of approximately 12 mm and a thickness of around 1.5 mm using a hydraulic press at 80 MPa. The PVB binder was burned off, and the pellets were sintered in air at 1,300°C for 2 h, with a heating rate of 5°C/min, and then allowed to cool naturally.

The phase formation of BCTS/MNZF ceramics was analyzed using X-ray diffraction (XRD, Bruker D8 Discover) with Cu Kα radiation, and the data were refined using the Rietveld method with FullProf software. The microstructure of the samples was examined using Field-Emission Scanning Electron Microscopy (FE-SEM, Thermo Fisher Scientific, Apreo S). For FE-SEM preparation, sintered pellets were polished with sandpaper and alumina abrasive, then thermal etching at 100°C below the sintering temperature for 30 min. Ceramic density was measured using the Archimedes method.

Dielectric properties were measured as a function of frequency at room temperature using an LCR analyzer (HP4284A, Hewlett-Packard, Palo Alto, CA, USA) over a frequency range of 100 Hz to 1 MHz. Polarization-electric field (P-E) hysteresis loops were recorded with a modified Sawyer-Tower circuit controlled by a computer (Radiant, PLC2-The P-E loop). Magnetic properties were assessed via a vibrating sample magnetometer (Versa Lab, Quantum Design), while the magnetoelectric coupling coefficient was determined with a lock-in amplifier (Stanford Research System, model SR830).

Results and Discussion

The X-ray diffraction (XRD) patterns of the (1-x)($Ba_{0.97}Ca_{0.03}Ti_{0.94}Sn_{0.06}O_3$)-x($Mn_{0.85}Ni_{0.15}Zn_{0.15}Fe_2O_4$) (x = 0.1, 0.2, 0.3, 0.4, and 0.5) ceramic samples are shown in Figure 1. The ferroelectric component exhibits a mixed-phase structure, consisting of both tetragonal perovskite (JCPDS: 74-1960) and orthorhombic perovskite structures (JCPDS: 81-1288), while the ferrite component shows a cubic spinel structure (JCPDS: 74-2403), similar to previous work (Chootin and Bongkarn, 2017; Jalaiah and Babu, 2017; Kornphom *et al*., 2018). As the ferrite content increased, more secondary phases of Mn_2O_3 (♥) and SnO (♣) tended to form. The main ferrite peak was observed at 2θ~35° and corresponds to the <311> plane. The intensity of the ferrite peak increases with the ferrite concentration.

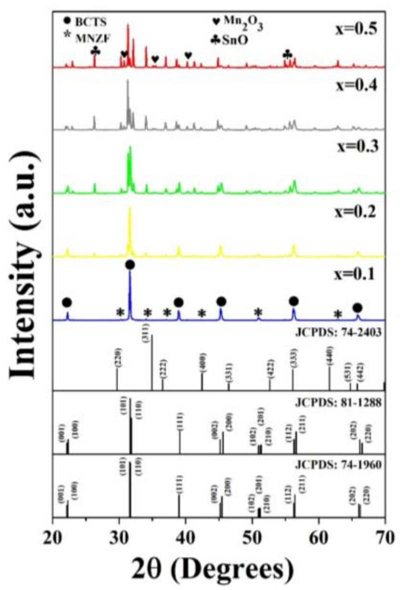

Figure 1. X-Ray diffraction patterns of BCTS/MNZF multiferroic composite ceramics with different MNZF concentrations

Figure 2 shows the FE-SEM images of the polished surfaces of BCTS/MNZF composite ceramics. The images reveal that porosity increases with rising ferrite content. For *x*≤0.2, the grains exhibit a hexagonal shape. As *x* increases, two distinct grain types appear in the FE-SEM images: hexagonal grains and rod-shaped grains (Figures 2(b–c)). A higher ferrite content leads to the appearance of more rod-shaped grains. Surface scanning using energy-dispersive spectroscopy

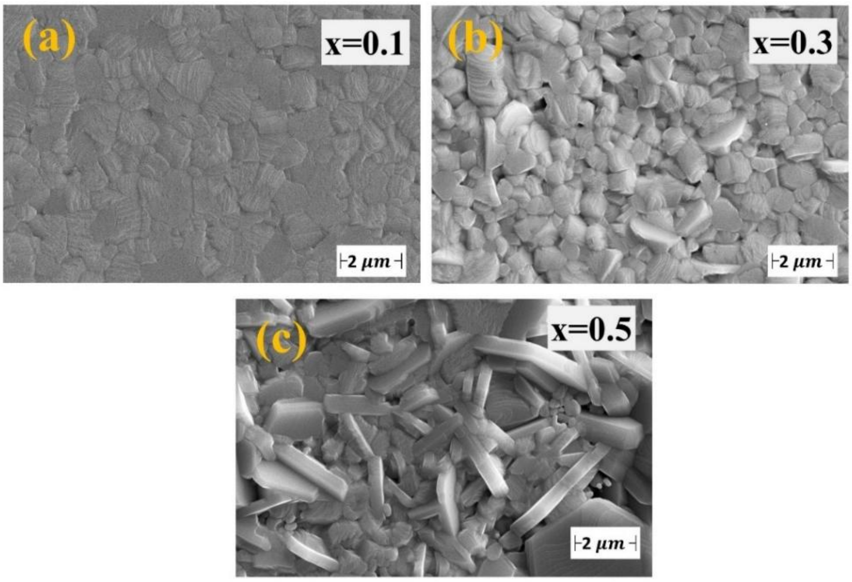

Figure 2. Microstructure of the BCTS/MNZF multiferroic composite ceramics with different MNZF concentrations (a) x = 0.1, (b) x = 0.3, and (c) x = 0.5

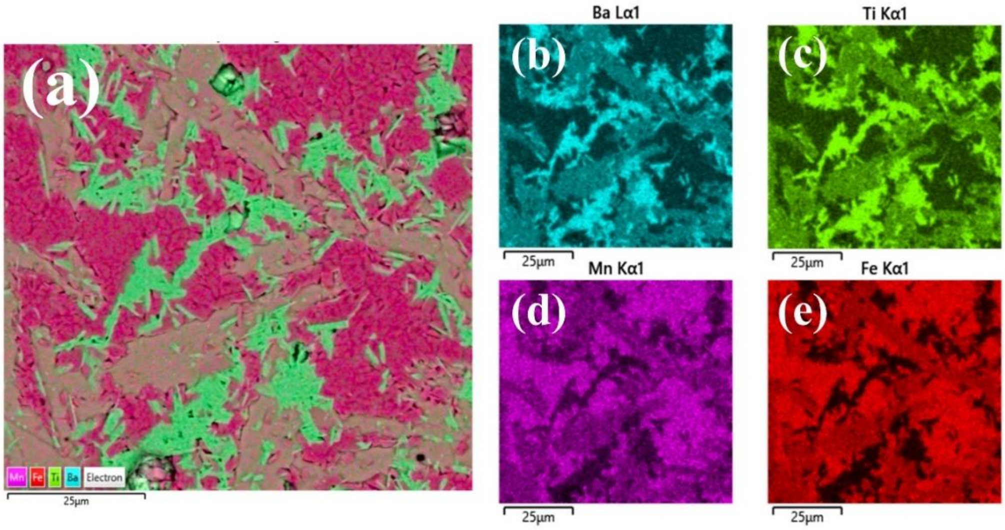

Figure 3. Results of surface scanning with energy dispersion technology (a) depicts the selected crystal region of BCTS/MNZF with x = 0.5, while (b)–(e) shows the distribution of the elements Ba, Ti, Mn, and Fe

(EDS) in the selected crystal area of the BCTS/MNZF composite at x = 0.5 is shown in Figure 3. It is evident from Figures 3b–c that Ba and Ti are uniformly dispersed in a thin layer, while Mn and Fe are highly concentrated across the sample, as seen in Figures 3(d–f).These results suggest that the hexagon shaped grains are BCTS, and the rod-shaped grains are MNZF. This distinction arises from the slower growth rate of the BCTS phase compared to the MNZF phase in the composite system (Pattanayak *et al*., 2017; Xiao *et al*., 2013; Zheng *et al*., 2009).

The black scattering mode of FE-SEM was employed to examine the grains. This technique highlights compositional variations based on differences in atomic number. Regions with heavier elements (higher atomic numbers) appear brighter, while areas with lighter elements appear darker (Kasperski *et al*., 2013). Figure 4 displays the FE-SEM image of the samples, where

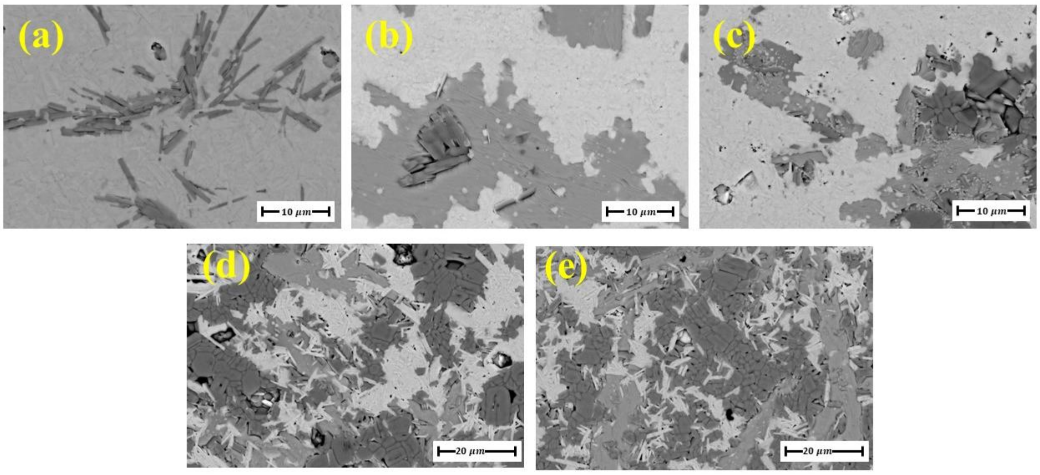

Figure 4. **FE-SEM image using black scattering mode of BCTS/MNZF multiferroic composite ceramics with different MNZF concentrations (a) x = 0.1, (b) x = 0.2, (c) x=0.3, (d) x = 0.4, and (e) x = 0.5**

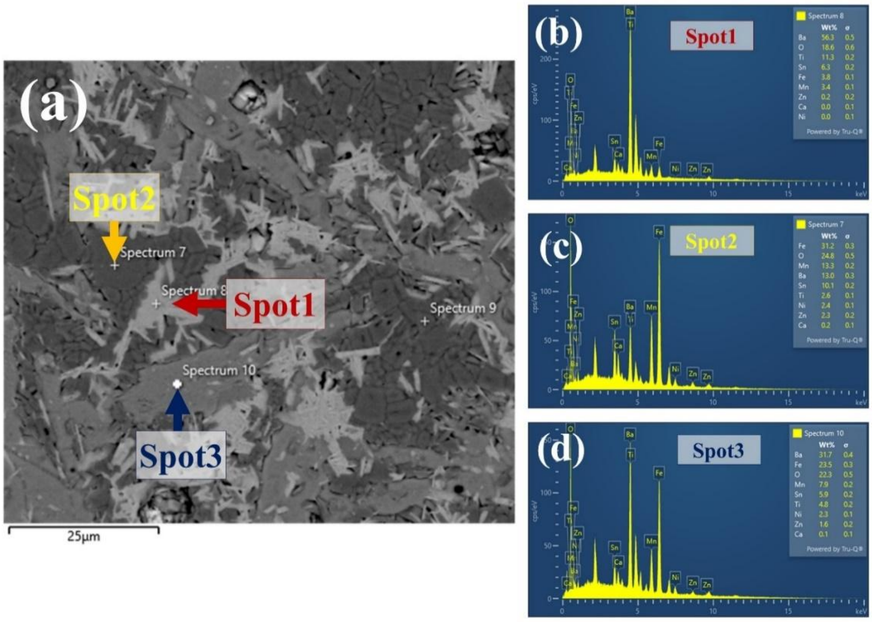

Figure 5. **presents the grain composition analysis results obtained using the Energy dispersion spectra (EDS) (a) depicts the selected crystal region of BCTS/MNZF with x=0.5, (b) EDS spectra at the bright grain, (c) EDS spectra at the black grain and (d) EDS spectra at the gray grain**

hexagonal, light-colored grains correspond to regions with high atomic numbers, while rod-shaped, dark-colored grains indicate areas with lower atomic numbers. An increase in ferrite content is associated with a notable growth in the dark regions.

Figure 5 presents the grain composition analysis results obtained using the Energy Dispersion Spectra (EDS) for the BCTS/MNZF sample at x = 0.5, based on data collected from three analyzed points (Figure 5(a)). Figure 5(b) presents the elemental percentage graph for the bright grain region, which reveals high concentrations of Ba, Ti, Sn, and Ca which corresponds to the perovskite phase. Figure 5c displays the elemental percentage graph for the black grain region, which is characterized by high concentrations of Mn and Fe, indicating the spinel ferrite phase. Figure 5(d)

Table 1. The average grain size, measured density, dielectric and magnetic properties of BCTS/MNZF ceramics

Content *x*	Density (g/cm^3)	Dielectric properties		Ferromagnetic properties			α_{ME} (mV/cm•Oe)
		Dielectric constant (ε) at 100 Hz	Dielectric Loss (tanδ) at 100 Hz	M_s (emu/g)	M_r (emu/g)	H_c (Oe)	
0.1	5.66	1,388	2.48	0.75	0.004	37.10	7.24
0.2	5.55	1,308	1.66	2.55	0.021	36.29	6.27
0.3	5.54	1,275	3.61	5.27	0.085	28.70	5.84
0.4	5.50	1,205	4.18	7.88	0.421	16.60	5.04
0.5	5.12	862	14.37	13.41	1.058	12.68	4.05

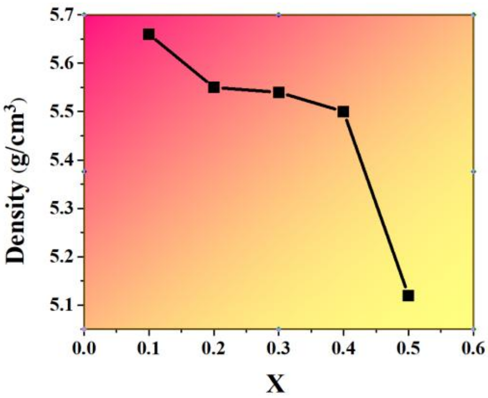

Figure 6. Variation of apparent density of BCTS/MNZF multiferroic composite ceramics as function of MNZF content

illustrates the elemental percentage graph for the gray grain region, showing a mixed composition high in Ba, Ti, Mn, and Fe (Phanjoubam *et al*., 1988). This mixed structure is because Fe^{3+} can easily diffuse into the BCTS structure, replacing Ti^{4+}, and Ti^{4+} can similarly diffuse into the MNZF structure, replacing Fe^{3+}, because of their similar electrovalence (Mudarra Navarro *et al*., 2019; Xiao *et al*., 2013).

The density of the BCTS/MZNF composite ceramics was measured using the Archimedes method, with the results shown in Figure 6. The density decreased from 5.66 g/cm^3 to 5.12 g/cm^3 as the ferrite content increased from x = 0.1 to x = 0.5 (Table 1). The maximum density of 5.66 g/cm^3 was observed for the composite with x = 0.1. Figures 2 and 6 demonstrated a similar pattern, where the average porosity and density declined as ferrite content rose. This result is attributed to increased grain shape heterogeneity, which contributed to the formation of voids and pores in the material.

Figure 7 shows the room-temperature frequency-dependent dielectric constant (ε) and dielectric loss (tanδ) of BCTS/MNZF composite ceramics sintered at 1,300°C. At lower frequencies, both ε and tanδ decreased sharply, but stabilized at higher frequencies (Zawar *et al*., 2019).

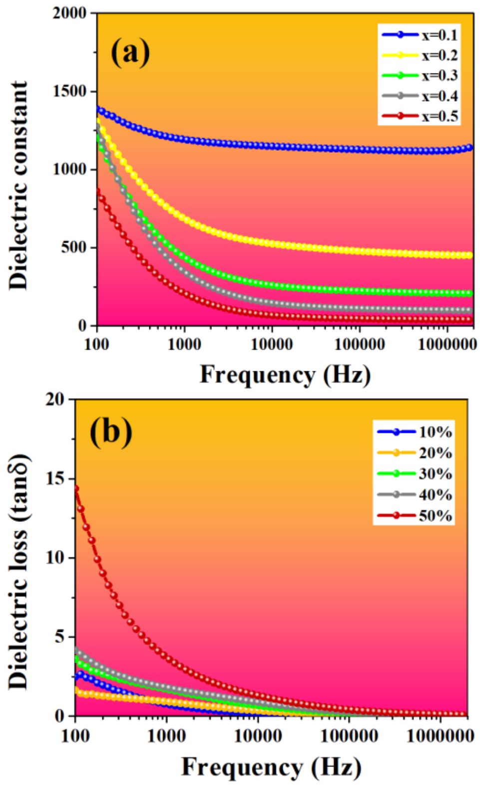

Figure 7. Frequency dependence of (a) the dielectric constant and (b) the dielectric loss measured at room temperature of the BCTS/MNZF multiferroic composite ceramics with different MNZF concentrations

The behavior of the dielectric constant and loss of composite materials decreasing with increasing frequency is due to the Maxwell-Wagner relaxation mechanism (Booth *et al*., 2015; Cañadilla *et al*., 2023). The dielectric constant reflects a material’s capacity to polarize under an external electric field, which is governed by several polarization mechanisms, including electronic, ionic, dipolar, and interfacial polarization. Each mechanism contributes to the material's overall dielectric behavior, influenced by its composition, structural characteristics, and the applied field frequency (McKeen, 2017). Electronic polarization is

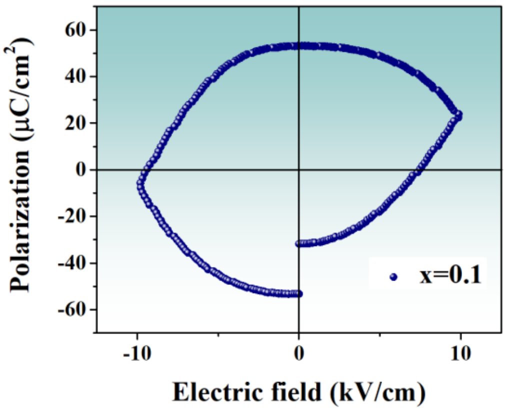

Figure 8. Polarization with different electric fields at frequency of 1 Hz of the BCTS/MNZF multiferroic composite ceramics with x = 0.1

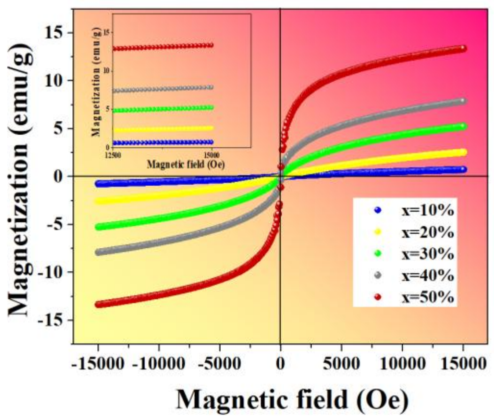

Figure 9. Ferromagnetic hysteresis (M-H) loops of BCTS/MNZF multiferroic composite ceramics with different MNZF concentrations

the dominate mechanism at elevated frequencies, as other polarization mechanisms become negligible, resulting in a reduction of the dielectric constant, as charge carriers cannot respond to the rapid electric field changes (Ahmed *et al*., 2013; Pahuja and Tandon, 2017).

From Table 1, increased ferrite content caused ε to decrease. This reduction is caused by the development of connected conductive pathways between ferrite particles as the ferrite concentration rises above the percolation threshold, enhancing charge transport, causing a lower ε (Venkata Ramana *et al*., 2010; Won *et al*., 2011). Increasing ferrite content (x) also increases the dielectric loss. This trend suggests that higher x leads to the formation of additional space charges, increased leakage current, and the presence of impurities within the ceramic structure. These factors contribute to the overall increase in dielectric loss (Gao *et al*., 2019).

The ferroelectric hysteresis loops of polarization versus electric field (P-E) for the BCTS/MNZF ceramics were measured under an electric field up to ±10 kV/cm. However, the only successful measurement was for x = 0.1due to short-circuit issues in other compositions. Figure 8 illustrates the P-E loop for x = 0.1, which is a broad loop with P_s = 23.95 μC/cm^2, P_r = 53.12 μC/cm^2, and E_c = 7.48 kV/cm. Compared to earlier findings of P_s ~20 μC/cm^2, P_r = 6.88 μC/cm^2, and E_c = 2.62 kV/cm (Chootin and Bongkarn, 2017), the results suggest that incorporating the ferrite phase increased the magnetic properties and altered the polarization behavior. The ferroelectric properties of the ferrite–piezoelectric composite ceramics are significantly influenced by the proportion of the ferromagnetic phase. As shown in Figure 8, the polarization remains unsaturated, with relatively low values, and the P–E loop displays an open-mouth characteristic as it approaches electrical breakdown. For compositions with x>0.1, polarization could not be achieved due to the conductive nature of the large MNZF grains, resulting in the masking of the electric polarization (Zhang *et al*., 2014; Gao *et al*., 2019).

The magnetic hysteresis loops of BCTS/MNZF composite ceramics were measured at room temperature, as shown in Figure 9. The loop exhibits a thin profile characteristic of soft magnets (Oikonomou, 2014). The values of saturation magnetization (M_s), remanent magnetization (M_r), and coercivity (H_c) were obtained from the hysteresis loops and are presented in Table 1. The M_s and M_r increased with the concentration of MNZF, from 0.75 to 13.41 emu/g and 0.004 to 1.058 emu/g, respectively. This increase is due to each MNZF grain serving as a magnetization center, and the total saturation magnetization of the composite is the cumulative vector sum of these individual contributions. Consequently, a higher ferrite content enhances magnetic ordering, increasing overall net magnetization (Grigalaitis *et al*., 2014; Rani *et al*., 2014). As the concentration of MNZF in multiferroic material increased, H_c decreased.

Figure 10 presents the magnetoelectric coupling coefficient (α_{ME}) under a DC magnetic field for the multiferroic BCTS-MNZF composite ceramics. As the ferrite content increases, the α_{ME} values at room temperature drop from 7.24 to 4.05 mV/cm·Oe, as indicated in Table 1. Due to its lower resistivity, the ferrite phase facilitates charge leakage from the piezoelectric grains through the low-resistance pathways provided by the

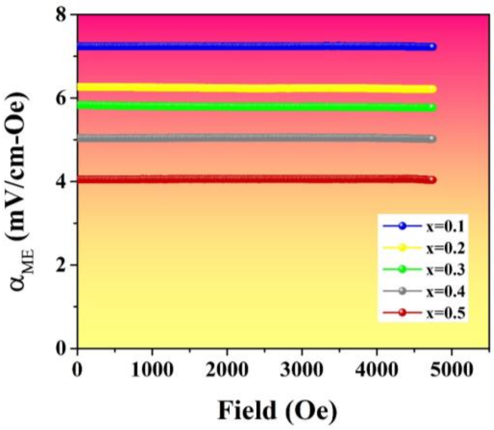

Figure 10. Variation of α_{ME} with H_{dc} measured at room temperature of BCTS/MNZF multiferroic composite ceramics with different MNZF concentrations

surrounding ferrite. Due to considerable charge leakage, excessive ferrite reduces the piezoelectric effect, lowering the magnetoelectric effect (Ahmed *et al.*, 2013; Rakhikrishna *et al.*, 2017; Sharma *et al.*, 2015). The two phases exhibit greater homogeneity as the value of x increases. The microstructure of the multiferroic materials achieves greater homogeneity when the components are thoroughly blended, leading to improved integration of the magnetic and ferroelectric phases. This uniformity enhancing both the magnetic properties and overall functional performance (Mitoseriu *et al.*, 2007). For x = 0.1, the uniform grain shape enhances magnetoelectric performance by reducing stress relaxation and improving interfacial coupling. A more homogeneous microstructure also reduces defects and irregularities, resulting in better phase interactions and a higher ME coefficient (Palneedi *et al.*, 2016; Viana *et al.*, 2022; Bochenek *et al.*, 2023).

Comparing the BCTS/MNZF ceramic composites' magnetic saturation (M_s) and magnetoelectric (α_{ME}) coupling values with those of lead-free multiferroic magnetoelectric materials from previous studies shows that the 5.5BCTS-4.5MNZF composites outperform others. In particular, their α_{ME} values exceed those of 0.65BSTH-0.35MZF (α_{ME} = 1.42 mV/cm·Oe) (Gao *et al.*, 2019), and their M_s values are higher than those of BT/MZF composites (M_s = 12.1 emu/g, H_c = 5.25 Oe) (Khader and Sankarappa, 2016). This suggests that the BCTS/MNZF ceramic composites have superior qualities that make them appropriate for various electronic device applications (Zhai *et al.*, 2006; Rahman *et al.*, 2013).

Conclusions

Magnetoelectric composites of BCTS and MNZF were synthesized using the solid-state combustion method. XRD analysis confirmed the formation of a two-phase composite structure consisting of perovskite and spinel phases. With increasing ferrite content, the density, dielectric constant, and magnetoelectric coefficient (α_{ME}) decreased from 5.66 to 5.12 g/cm³, 1,388 to 862, and 7.24 to 4.05 mV/cm·Oe, respectively, while the saturation magnetization (M_s) significantly increased from 0.75 to 13.14 emu/g. The optimal composition for BCTS/MNZF ceramics was found at x = 0.4, offering balanced properties including high density, excellent dielectric performance (ε = 1,205 and tanδ = 4.18), favorable magnetic characteristics (M_s = 7.88 emu/g, M_r = 0.421 emu/g, and H_c = 16.60 Oe), and a good α_{ME} value of 5.04 mV/cm·Oe. These composites exhibit superior dielectric and magnetoelectric coupling properties, making them highly suitable for applications in inductors, resistors, and capacitors over a wide frequency range.

Acknowledgement

The research was funded by Faculty of Science, Naresuan University. The work of Nutkamon Sonchaopri was supported by National Research Council of Thailand (NRCT) with Grant No. N41A661124. The authors would also like thank Asst. Prof. Dr. Kyle V. Lopin for his help with improving the manuscript.

References

Ahmed, M., Mansour, S., and Abdo, M. (2013). Improvement of the physical properties of novel (1−y)$Co_{0.8}Cu_{0.2}Fe_2O_4$+(y)$SrTiO_3$ nanocomposite. Materials Research Bulletin, 48(5):1796–1805. https://doi.org/10.1016/j.materresbull.2013.01.034

Angadi, V.J., Choudhury, L., Sadhana, K., Liu, H.-L., Sandhya, R., Matteppanavar, S., Rudraswamy, B., Pattar, V., Anavekar, R., and Praveena, K. (2017). Structural, electrical and magnetic properties of Sc^{3+} doped Mn-Zn ferrite nanoparticles. Journal of Magnetism and Magnetic Materials, 424:1–11. https://doi.org/10.1016/j.jmmm.2016.10.050

Bochenek, D., Niemiec, P., Chrobak, A., and Guzdek, P. (2023). Magnetoelectric properties of multiferroic ceramic composites. Applied Physics A, 129:642. https://doi.org/10.1007/s00339-023-06921-6

Booth, F.N., Garrido, L.B., and Aglietti, E.F. (2015). Effect of impurities and sintering temperature on properties of MgO-$CaZrO_3$ ceramics. Procedia Materials Science, 8:172–179. https://doi.org/10.1016/j.mspro.2015.04.061

Cañadilla, A., Sanhueza, J.P., Montalba, C., and Ruiz-Navas, E.M. (2023). Effect of sintering temperature on phase formation and mechanical properties of Al-Cu-Li alloy prepared from secondary aluminum powders. Metals, 14(1):12. https://doi.org/10.3390/met14010012

Chen, X., Xiao, J., Yao, J., Kang, Z., Yang, F., and Zeng, X. (2014). Room temperature magnetoelectric coupling study in multiferroic $Bi_4NdTi_3Fe_{0.7}Ni_{0.3}O_{15}$ prepared by a multicalcination procedure. Ceramics International, 40:6815–6819. https://doi.org/10.1016/j.ceramint.2013.11.144

Chootin, S. and Bongkarn, T. (2017). Optimum conditions for preparation of high-performance $(Ba_{0.97}Ca_{0.03})(Ti_{0.94}Sn_{0.06})O_3$ ceramics by solid-state combustion. Journal of Electronic Materials, 46:5215–5224. https://doi.org/10.1007/s11664-017-5533-6

Dastjerdi, O.D., Shokrollahi, H., and Mirshekari, S. (2023). A review of synthesis, characterization, and magnetic properties of soft spinel ferrites. Inorganic Chemistry Communications, 153:110797. https://doi.org/10.1016/j.inoche.2023.110797

Fawzi, A.S., Sheikh, A.D., and Mathe, V.L. (2010). Dielectric, electrical and magnetoelectric characterization of $(x)Ni_{0.8}Zn_{0.2}Fe_2O_4+(1-x)Pb_{0.93}La_{0.07}(Zr_{0.60}Ti_{0.40})O_3$ composites. Materials Research Bulletin, 45(8):1000–1007. https://doi.org/10.1016/j.materresbull.2010.04.005

Gao, R., Qin, X., Zhang, Q., Xu, Z., Wang, Z., Fu, C., Chen, G., Deng, X., and Cai, W. (2019). Enhancement of magnetoelectric properties of $(1-x)Mn_{0.5}Zn_{0.5}Fe_2O_4$–$xBa_{0.85}Sr_{0.15}Ti_{0.9}Hf_{0.1}O_3$ composite ceramics. Journal of Alloys and Compounds, 795:501–512. https://doi.org/10.1016/j.jallcom.2019.05.013

Grigalaitis, R., Petrović, M.M.V., Bobić, J.D., Dzunuzovic, A., Sobiestianskas, R., Brilingas, A., Stojanović, B.D., and Banys, J. (2014). Dielectric and magnetic properties of $BaTiO_3$–$NiFe_2O_4$ multiferroic composites. Ceramics International, 40:6165–6170. https://doi.org/10.1016/j.ceramint.2013.11.069

Haralkar, S.J., Kadam, R.H., More, S.S., Shirsath, S.E., Mane, M.L., Patil, S., and Mane, D.R. (2013). Intrinsic magnetic, structural and resistivity properties of ferromagnetic $Mn_{0.5}Zn_{0.5}Al_xFe_{2-x}O_4$ nanoparticles. Materials Research Bulletin, 48(3):1189–1196. https://doi.org/10.1016/j.materresbull.2012.12.018

Islam, R., Hakim, MA. Rahman, M.O., Das, H.N., and Mamun, M.A. (2013). Study of the structural, magnetic and electrical properties of Gd-substituted Mn-Zn mixed ferrites. Journal of Alloys and Compounds, 559:174–180. https://doi.org/10.1016/j.jallcom.2012.12.080

Jalaiah, K. and Babu, K.V. (2017). Structural, magnetic and electrical properties of nickel doped Mn-Zn spinel ferrite synthesized by sol-gel method. Journal of Magnetism and Magnetic Materials, 423:275–280. https://doi.org/10.1016/j.jmmm.2016.09.114

Kasperski, A., Weibel, A., Estournès, C., Laurent, C., and Peigney, A. (2013). Preparation-microstructure-property relationships in double-walled carbon nanotubes/alumina composites. Carbon, 53:62–72. https://doi.org/10.1016/j.carbon.2012.10.030

Khader, S.A. and Sankarappa, T. (2016). Dielectric, magnetic and ferroelectric studies in $(x)Mn_{0.5}Zn_{0.5}Fe_2O_4+(1-x)BaTiO_3$ magnetoelectric nano-composites. Materials Today: Proceedings, 3(6):2358–2365. https://doi.org/10.1016/j.matpr.2016.04.148

Kornphom, C., Yotthuan, S., Chootin, S., and Bongkarn, T. (2018). The influence of the firing temperatures on the phase evolution, microstructure, dielectric and strain responses of BCTS ceramics prepared by the solid state combustion technique. Physica Status Solidi (a), 215(21):1701058. https://doi.org/10.1002/pssa.201701058

Latorre-Esteves, M., Cortes, A., Torres-Lugo, M., and Rinaldi, C. (2009). Synthesis and characterization of carboxymethyl dextran-coated Mn/Zn ferrite for biomedical applications. Journal of Magnetism and Magnetic Materials, 321(19):3061–3066. https://doi.org/10.1016/j.jmmm.2009.05.023

Leung, C.M., Li, J., Viehland, D., and Zhuang, X. (2018). A review on applications of magnetoelectric composites: From heterostructural uncooled magnetic sensors, energy harvesters to highly efficient power converters. Journal of Physics D: Applied Physics, 51:263002. https://doi.org/10.1088/1361-6463/aac60b

Matavž, A., Koželj, P., Winkler, M., Geirhos, K., Lunkenheimer, P., and Bobnar, V. (2021). Nanostructured multiferroic $Pb(Zr,Ti)O_3$–$NiFe_2O_4$ thin-film composites. Thin Solid Films, 732:138740. https://doi.org/10.1016/j.tsf.2021.138740

McKeen, L.W. (2017). Film Properties of Plastics and Elastomers. 4th ed. William Andrew, 522p.

Mitoseriu, L., Pallecchi, I., Buscaglia, V., Testino, A., Ciomaga, C.E., and Stancu, A. (2007). Magnetic properties of the $BaTiO_3$–$(Ni,Zn)Fe_2O_4$ multiferroic composites. Journal of Magnetism and Magnetic Materials, 316(2):e603–e606. https://doi.org/10.1016/j.jmmm.2007.03.036

Mudarra Navarro, A.M., Gil Rebaza, A.V., Salcedo Rodriguez, K.L., Melo Quintero, J.J., Rodríguez Torres, C.E., Weissmann, M., and Errico, L.A. (2019). Structural, electronic, and magnetic properties and hyperfine interactions at the Fe sites of the spinel $TiFe_2O_4$. Ab initio, XANES, and Mossbauer study. The Journal of Physical Chemistry C, 123(35):21694–21703. https://doi.org/10.1021/acs.jpcc.9b06550

Navadeepthy, D., Srividhya, G., and Ponpandian, N. (2022). Synthesis of magnetoelectric multiferroics and its composites. In: Handbook of Magnetic Hybrid Nanoalloys and their Nanocomposites, Springer, p. 1–30. https://doi.org/10.1007/978-3-030-34007-0_10-1

Oikonomou, C. (2014). Surface characterization of soft magnetic composite powder and compacts, [Doctoral dissertation]. Department of Materials and Manufacturing Technology, Chalmers University of Technology, Gothenburg, Sweden, 48p.

Ortega, N., Kumar, A., Scott, J.F., and Katiyar, R.S. (2015). Multifunctional magnetoelectric materials for device applications. Journal of Physics: Condensed Matter, 27:504002. https://doi.org/10.1088/0953-8984/27/50/504002

Pahuja, P. and Tandon, R. (2017). Structural and dielectric properties of multiferroic composite system $Ba_{0.5}Sr_{0.5}TiO_3$–$Ni_{0.4}Co_{0.2}Zn_{0.4}Fe_2O_4$. Ferroelectrics, 516(1):122–126. https://doi.org/10.1080/00150193.2017.1362295

Palneedi, H., Annapureddy, V., Priya, S., and Ryu, J. (2016). Status and perspectives of multiferroic magnetoelectric composite materials and applications. Actuators, 5(1):9. https://doi.org/10.3390/act5010009

Pattanayak, R., Kuila, S., Raut, S., Ghosh, S.P., Dhal, S., and Panigrahi, S. (2017). Observation of grain size effect on multiferroism and magnetoelectric coupling of $Na_{0.5}Bi_{0.5}TiO_3$–$BaFe_{12}O_{19}$ novel composite system. Journal of Magnetism and Magnetic Materials, 444:401–409. https://doi.org/10.1016/j.jmmm.2017.08.048

Phanjoubam, S., Kothari, D., Baijal, J., and Kishan, P. (1988). Effect of Ti^{4+} substitution on the hyperfine interactions in LiZn ferrites. Solid State Communications, 68(6):549–554. https://doi.org/10.1016/0038-1098(88)90201-3

Rahman, M.A., Gafur, M., and Hossain, A.A. (2013). Structural, magnetic and transport properties of magnetoelectric composites. Journal of Magnetism and Magnetic Materials, 345:89–95. https://doi.org/10.1016/j.jmmm.2013.06.004

Rakhikrishna, R., Isaac, J., and Philip, J. (2017). Magneto-electric coupling in multiferroic nanocomposites of the type $x(Na_{0.5}K_{0.5})_{0.94}Li_{0.06}NbO_3$–$(1-x)CoFe_2O_4$: Role of ferrite phase. Ceramics International, 43(1 Part A):664–671. https://doi.org/10.1016/j.ceramint.2016.09.212

Ramana, M.V., Reddy, N.R., Murty, B.S., Murthy, V.R.K., and Kumar, K.V.S. (2010). Ferromagnetic-dielectric $Ni_{0.5}Zn_{0.5}Fe_{1.9}O_{4-\delta}/PbZr_{0.52}Ti_{0.48}O_3$ particulate composites: Electric, magnetic, mechanical, and electromagnetic properties. Advances in Condensed Matter Physics, 2010:763406. https://doi.org/10.1155/2010/763406

Rani, J., Yadav, K., and Prakash, S. (2014). Dielectric and magnetic properties of $xCoFe_2O_4$–(1−x)[0.5Ba $(Zr_{0.2}Ti_{0.8})O_3$–0.5$(Ba_{0.7}Ca_{0.3})TiO_3$] composites. Materials Research Bulletin, 60:367–375. https://doi.org/10.1016/j.materresbull.2014.09.013

Scott, J. (2007). Multiferroic memories. Nature Materials, 6:256–257. https://doi.org/10.1038/nmat1868

Scott, J.F. (2013). Room-temperature multiferroic magnetoelectrics. NPG Asia Materials, 5:e72. https://doi.org/10.1038/am.2013.58

Sharma, R., Singh, V., Kotnala, R.K., and Tandon, R.P. (2015). Investigation on the effect of ferrite content on the multiferroic properties of (1–x)$Ba_{0.95}Sr_{0.05}TiO_3$(x) $Ni_{0.7}Zn_{0.2}Co_{0.1}Fe_2O_4$ ceramic composite. Materials Chemistry and Physics, 160:447–455. https://doi.org/10.1016/j.matchemphys.2015.05.019

Thakur, P., Chahar, D., Taneja, S., Bhalla, N., and Thakur, A. (2020). A review on MnZn ferrites: Synthesis, characterization and applications. Ceramics International, 46(10 Part B):15740–15763. https://doi.org/10.1016/j.ceramint.2020.03.287

Verma, A., Alam, M.I., Chatterjee, R., Goel, T.C., and Mendiratta, R.G. (2006). Development of a new soft ferrite core for power applications. Journal of Magnetism and Magnetic Materials, 300(2):500–505. https://doi.org/10.1016/j.jmmm.2005.05.040

Viana, D.S.F., De Oliveira, A.J.A., Jimenez, K.R.C.P., Milton, F.P., Eiras, J.A., Santos, G.M., and Garcia, D. (2022). Synthesis and multiferroic properties of particulate composites resulting from combined size effects of the magnetic and ferroelectric phases. Ceramics International, 48(1):931–940. https://doi.org/10.1016/j.ceramint.2021.09.177

Wang, Z., Gao, R., Chen, G., Deng, X., Cai, W., and Fu, C. (2020). Dielectric, ferroelectric and magnetoelectric properties of in-situ synthesized $CoFe_2O_4/BaTiO_3$ composite ceramics. Ceramics International, 46(7):9154–9160. https://doi.org/10.1016/j.ceramint.2019.12.165

Won, C., Kambale, R., and Hur, N. (2011). Magnetic and transport properties of Ni_2MnGa–$BaTiO_3$ metal–insulator particulate composite with percolation threshold. Journal of Alloys and Compounds, 509(24):6969–6972. https://doi.org/10.1016/j.jallcom.2011.04.020

Xiao, B., Dong, Y., Ma, N., and Du, P. (2013). Formation of sol–gel in situ derived BTO/NZFO composite ceramics with considerable dielectric and magnetic properties. Journal of the American Ceramic Society, 96(4):1240–1247. https://doi.org/10.1111/jace.12181

Yadav, N., Kumar, A., Rana, P.S., Rana, D.S., Arora, M., and Pant, R.P. (2015). Finite size effect on Sm^{3+} doped $Mn_{0.5}Zn_{0.5}Sm_xFe_{2-x}O_4$ ($0 \leq x \leq 0.5$) ferrite nanoparticles. Ceramics International, 41(7):8623–8629. https://doi.org/10.1016/j.ceramint.2015.03.072

Zawar, S., Atiq, S., Tabasum, M., Riaz, S., and Naseem, S. (2019). Highly stable dielectric frequency response of chemically synthesized Mn-substituted $ZnFe_2O_4$. Journal of Saudi Chemical Society, 23(4):417–426. https://doi.org/10.1016/j.jscs.2018.06.010

Zhai, J., Xing, Z., Dong, S., Li, J., and Viehland, D. (2006). Detection of pico-Tesla magnetic fields using magneto-electric sensors at room temperature. Applied Physics Letters, 88(6):062510. https://doi.org/10.1063/1.2172706

Zhang, R.-F., Deng, C.-Y., Ren, L., Li, Z., and Zhou, J.-P. (2014). Ferroelectric, ferromagnetic, and magnetoelectric properties of multiferroic $Ni_{0.5}Zn_{0.5}Fe_2O_4$–$BaTiO_3$ composite ceramics. Journal of Electronic Materials, 43(4):1043–1047. https://doi.org/10.1007/s11664-013-2904-5

Zheng, H., Dong, Y., Wang, X., Weng, W., Han, G., Ma, N., and Du, P. (2009). Super high threshold percolative ferroelectric/ferrimagnetic composite ceramics with outstanding permittivity and initial permeability. Angewandte Chemie International Edition, 48(47):8927–8930. https://doi.org/10.1002/anie.200904269